Supplement of Atmos. Chem. Phys., 25, 16817–16832, 2025
https://doi.org/10.5194/acp-25-16817-2025-supplement

Atmospheric Chemistry and Physics
Open Access

Supplement of

Photochemical processing of dissolved organic matter in fog water: oxidation and functionalization pathways driving organic aerosol evolution

Wenqing Jiang et al.

Correspondence to: Qi Zhang (dkwzhang@ucdavis.edu)

Table S1. Chemical composition of the three fog samples combined for photochemical experiments in this study

Three fog samples collected on 1/9/2010 1:30 - 8:30		
Average Concentration ($mg\ L^{-1}$)[a]		pH[a]
Sulfate	9.51	6.98 - 7.37
Ammonium	23.4	
Nitrate	40.49	
Chloride	0.75	
Organics	23.08[b]	

a. Values are derived from Kim et al. (2019)

b. Calculated from DOC concentration (13.42 $mgC\ L^{-1}$) and HR-AMS measured OM/OC (≈1.72)

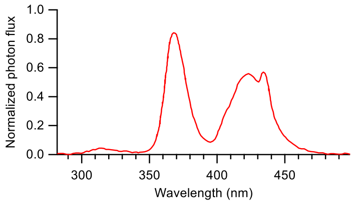

Figure S1. Normalized distribution of the photon fluxes inside the RPR-200 illumination system (George et al., 2015; Jiang et al., 2021)

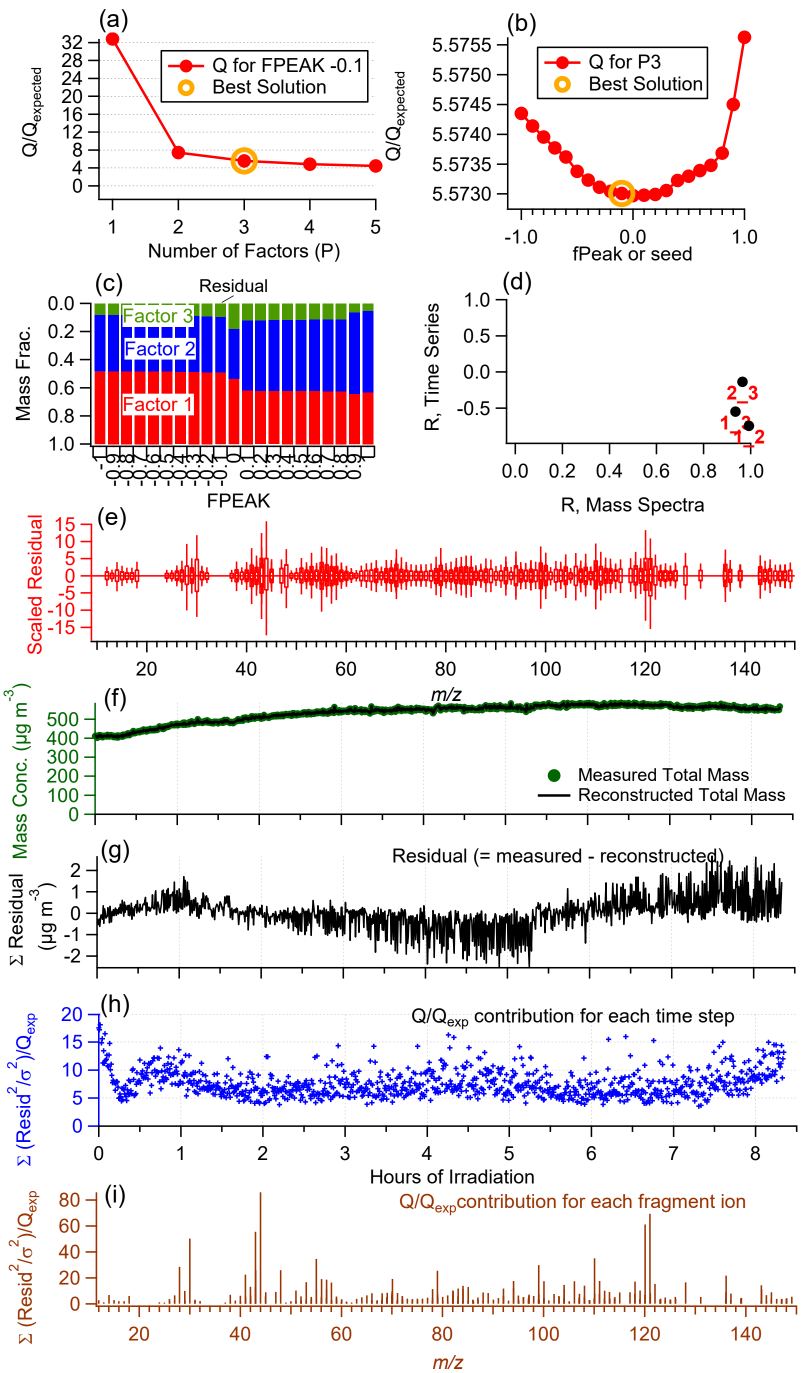

Figure S2. Summary of key diagnostic plots of the PMF results: **(a)** Q/Q_{exp} as a function of number of factors (p) selected for PMF analysis. For the best solution (3-factor solution) **(b)** Q/Q_{exp} as a function of *fPeak*, **(c)** fractions of PMF factors *vs*. *fPeak*, **(d)** correlations among PMF factors, **(e)** the box and whiskers plot showing the distributions of scaled residuals for each *m/z*, **(f)** time series of the measured organic mass and the reconstructed organic mass, **(g)** variations of the residual (= measured - reconstructed) of the fit, **(h)** the Q/Q_{exp} for each point in time, and **(i)** the Q/Q_{exp} values for each ion.

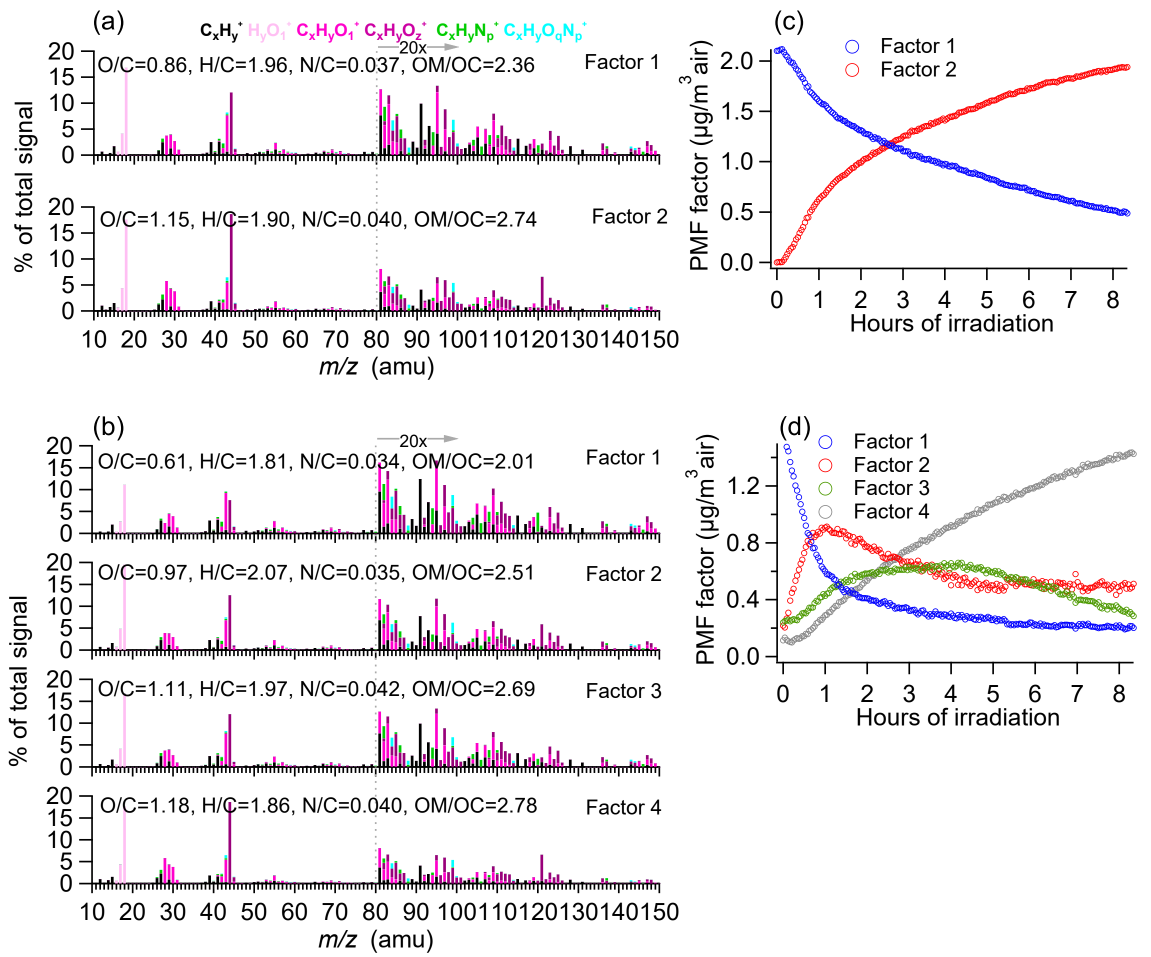

Figure S3. HR-AMS spectra for **(a)** two-factor PMF solutions and **(b)** four-factor PMF solutions. Peaks are colored by the six ion categories: $C_xH_y^+$, $H_yO_1^+$, $C_xH_yO_1^+$, $C_xH_yO_z^+$, $C_xH_yN_p^+$, and $C_xH_yO_qN_p^+$. The ion signals at $m/z_{\geq 80}$ are enhanced by a factor of 20 for clarity. The calculated atomic ratios are shown in the legends. Time series of **(c)** two-factor PMF solutions and **(d)** four-factor PMF solutions.

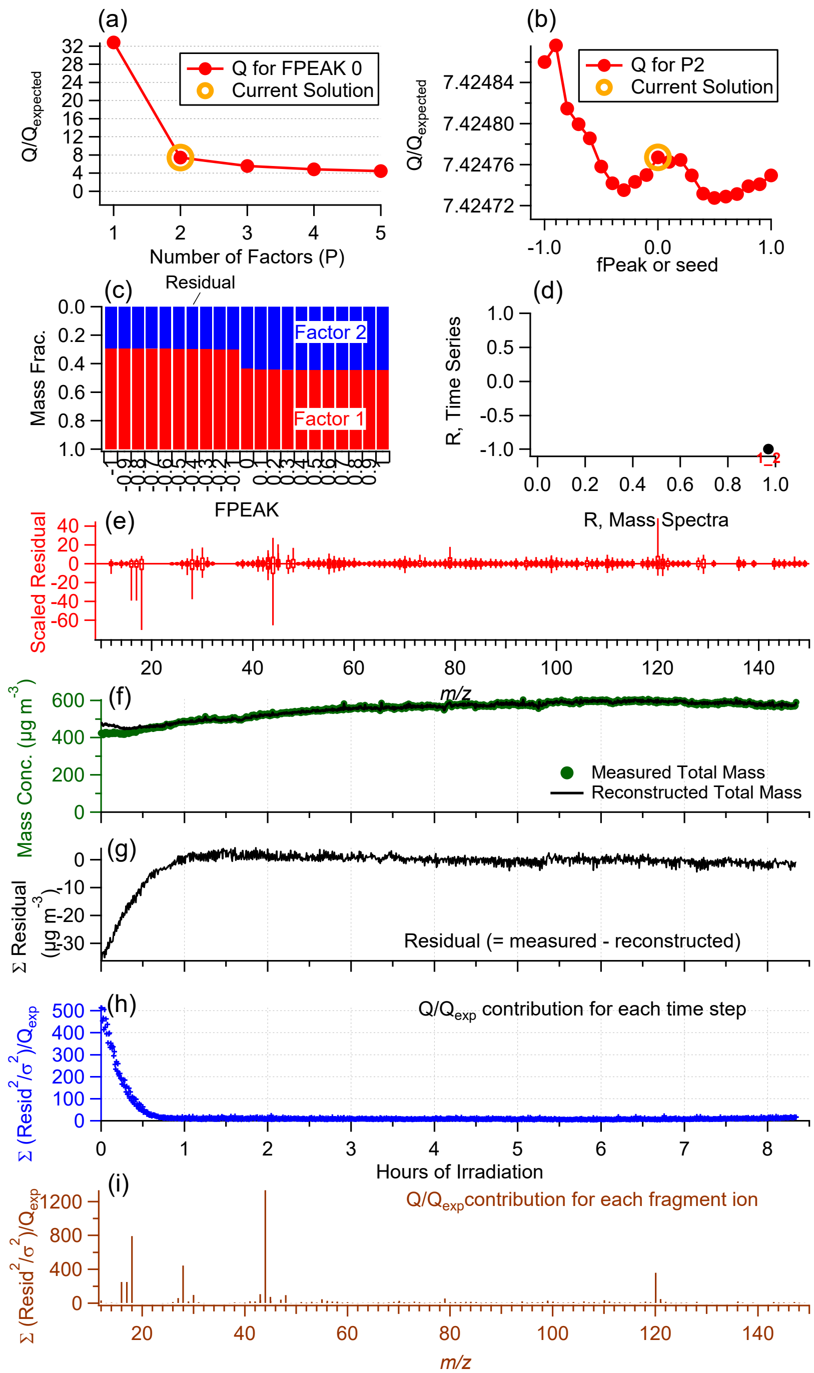

Figure S4. Summary of key diagnostic plots of the PMF results: **(a)** Q/Q_{exp} as a function of number of factors (p) selected for PMF analysis. For the 2-factor solution **(b)** Q/Q_{exp} as a function of *fPeak*, **(c)** fractions of PMF factors *vs*. *fPeak*, **(d)** correlations among PMF factors, **(e)** the box and whiskers plot showing the distributions of scaled residuals for each *m/z*, **(f)** time series of the measured organic mass and the reconstructed organic mass, **(g)** variations of the residual (= measured - reconstructed) of the fit, **(h)** the Q/Q_{exp} for each point in time, and **(i)** the Q/Q_{exp} values for each ion.

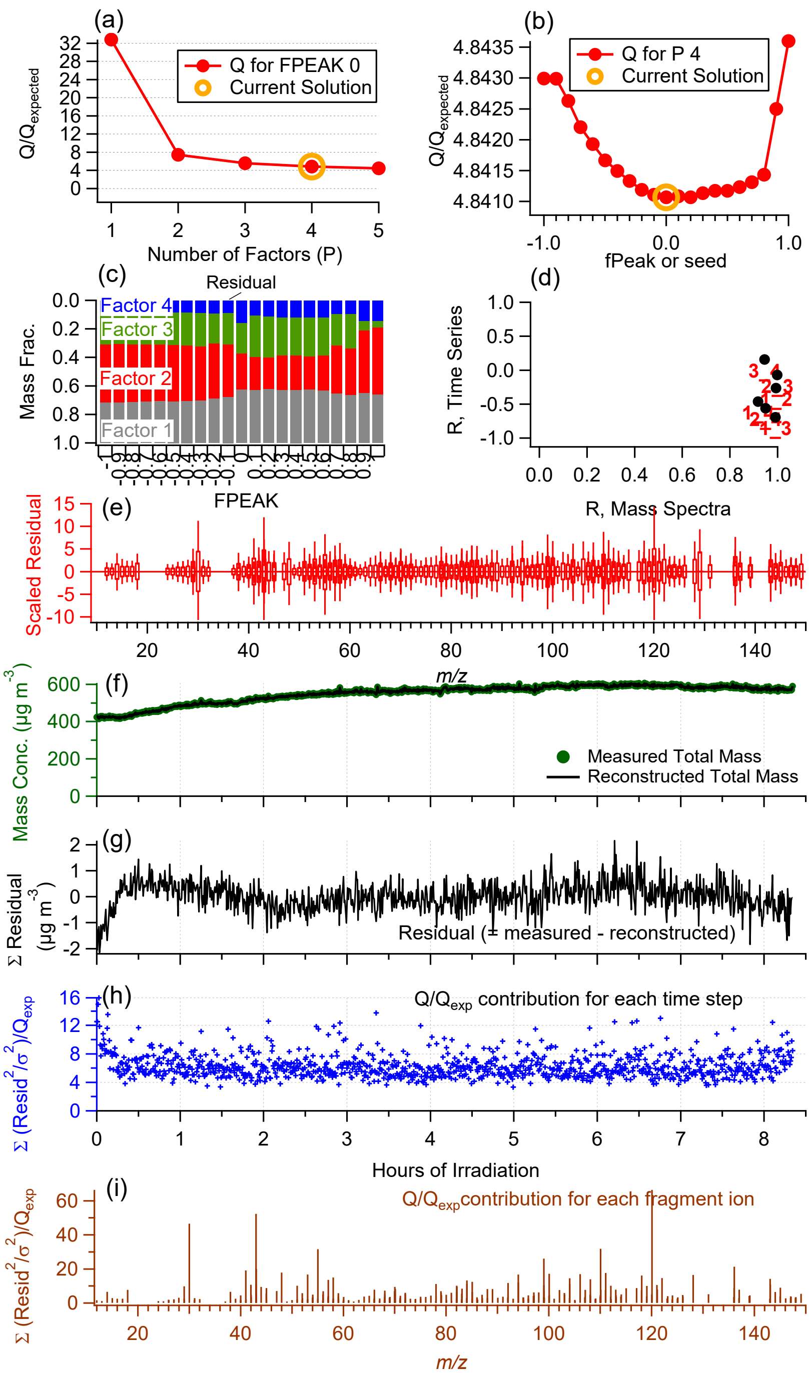

Figure S5. Summary of key diagnostic plots of the PMF results: **(a)** Q/Q_{exp} as a function of number of factors (*p*) selected for PMF analysis. For the 4-factor solution **(b)** Q/Q_{exp} as a function of *fPeak*, **(c)** fractions of PMF factors *vs*. *fPeak*, **(d)** correlations among PMF factors, **(e)** the box and whiskers plot showing the distributions of scaled residuals for each *m/z*, **(f)** time series of the measured organic mass and the reconstructed organic mass, **(g)** variations of the residual (= measured - reconstructed) of the fit, **(h)** the Q/Q_{exp} for each point in time, and **(i)** the Q/Q_{exp} values for each ion.

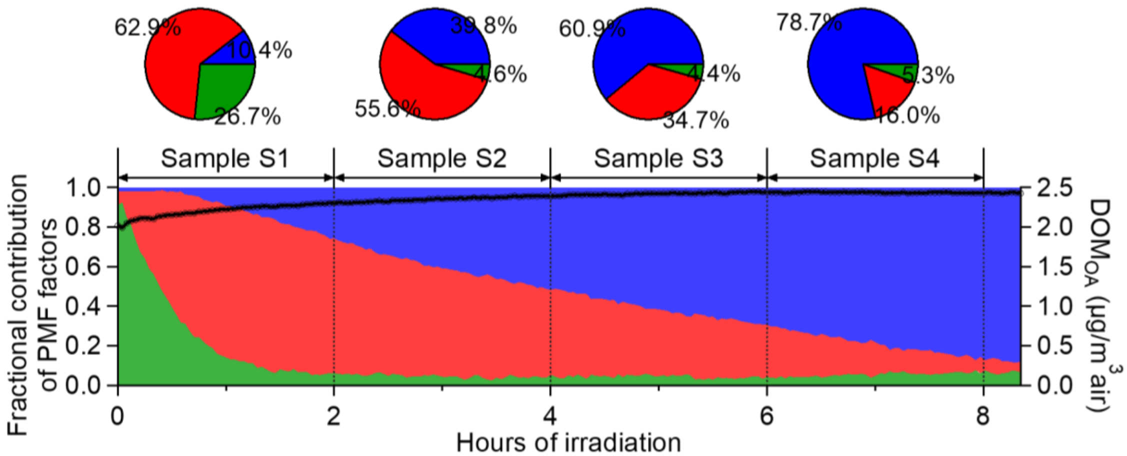

Figure S6. Fractional contributions of different PMF factors (from the 3-factor PMF solution) to DOM_{OA} in fog water samples collected at four irradiation intervals: S1 (0 – 2h), S2 (2-4 h), S3 (4-6 h) and S4 (6-8 h).

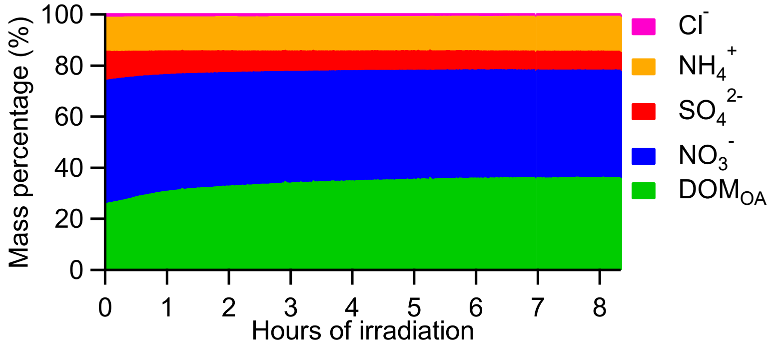

Figure S7. Mass fractions of major inorganic species and DOM_{OA} during fog water photochemical aging

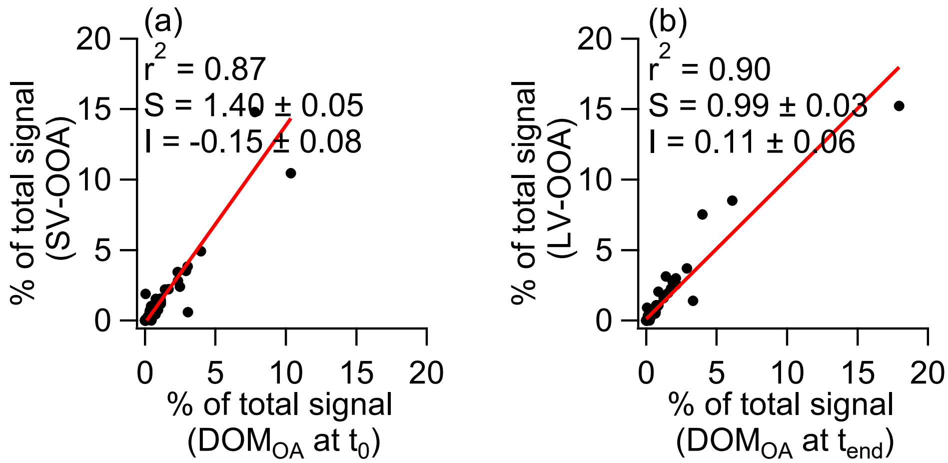

Figure S8. Scatter plots that compare the mass spectrum of SV-OOA and LV-OOA observed in ambient aerosols in Fresno in 2013 with the mass spectra of DOM_{OA} at t_0 and t_{end}, respectively. All linear regressions were performed using orthogonal distance regression (ODR) and the slopes (S), intercepts (I), and correlation coefficients (r^2) are shown in the legends.

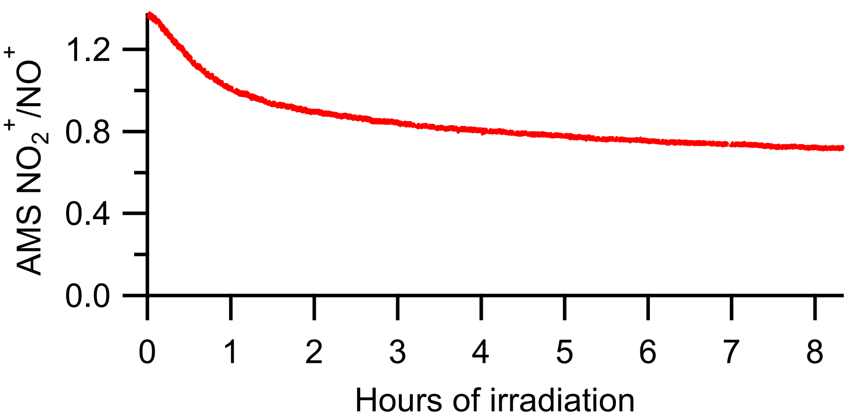

Figure S9. AMS NO_2^+/NO^+ ratio of the fog sample during photochemical aging

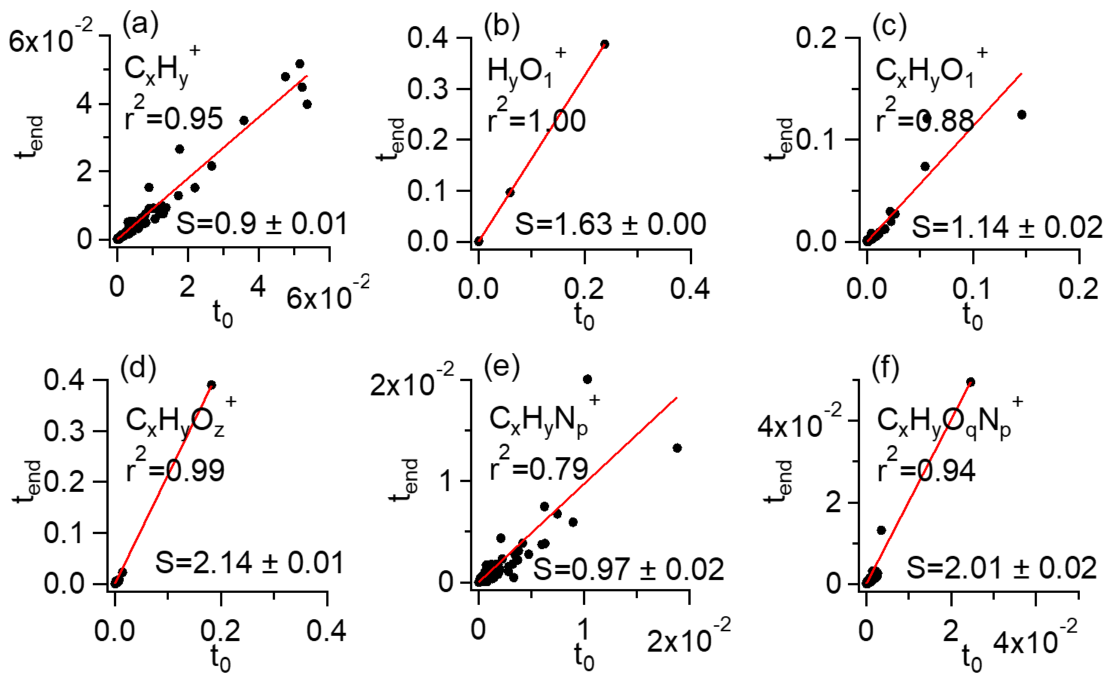

Figure S10. Comparison of the absolute signal intensities of organic AMS ion categories (i.e., $C_xH_y^+$, $H_yO_1^+$, $C_xH_yO_1^+$, $C_xH_yO_z^+$, $C_xH_yN_p^+$, and $C_xH_yO_qN_p^+$ ($x \geq 1$; $y \geq 1$; $z > 1$; $p \geq 1$; $q \geq 1$)) at t_0 and t_{end}. Red lines show orthogonal distance regression (ODR) fits; slopes (S) and correlation coefficients (r^2) are provided in each panel.

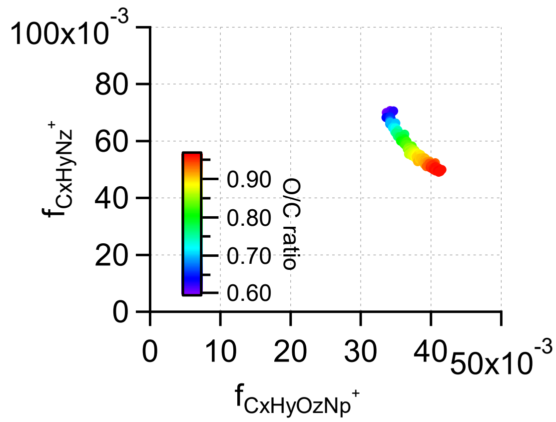

Figure S11. Evolution of the relationship between AMS-measured $C_xH_yN_p^+$ and $C_xH_yO_qN_p^+$ ion categories' fractional contributions, reflecting oxidative transformation of nitrogen-containing species.

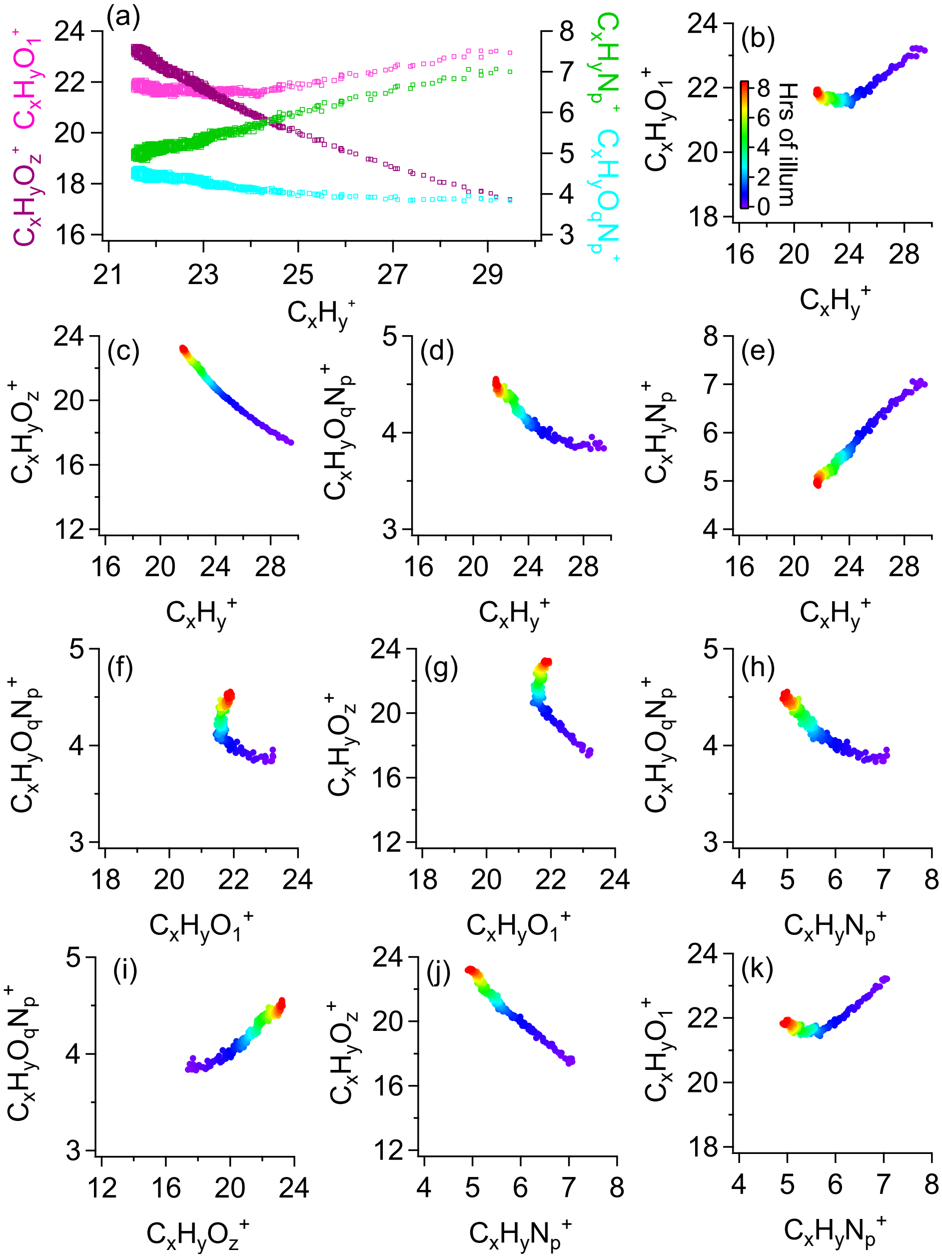

Figure S12. Correlations among signal contributions of major ion categories to DOM_{OA} spectra during simulated sunlight illumination. **(a)** Signal contributions (%) of $C_xH_yO_1^+$, $C_xH_yO_z^+$, $C_xH_yN_p^+$, and $C_xH_yO_qN_p^+$ plotted against $C_xH_y^+$ ($x \geq 1$; $y \geq 1$; $z > 1$; $p \geq 1$; $q \geq 1$). Each ion category is shown in a different color and symbol size scaled to irradiation time. **(b-k)** Pairwise correlations between the signal contributions (%) of $C_xH_yO_1^+$, $C_xH_yO_z^+$, $C_xH_yN_p^+$, $C_xH_yO_qN_p^+$, and $C_xH_y^+$. Data points are color-coded by hours of illumination (see color bar in b).

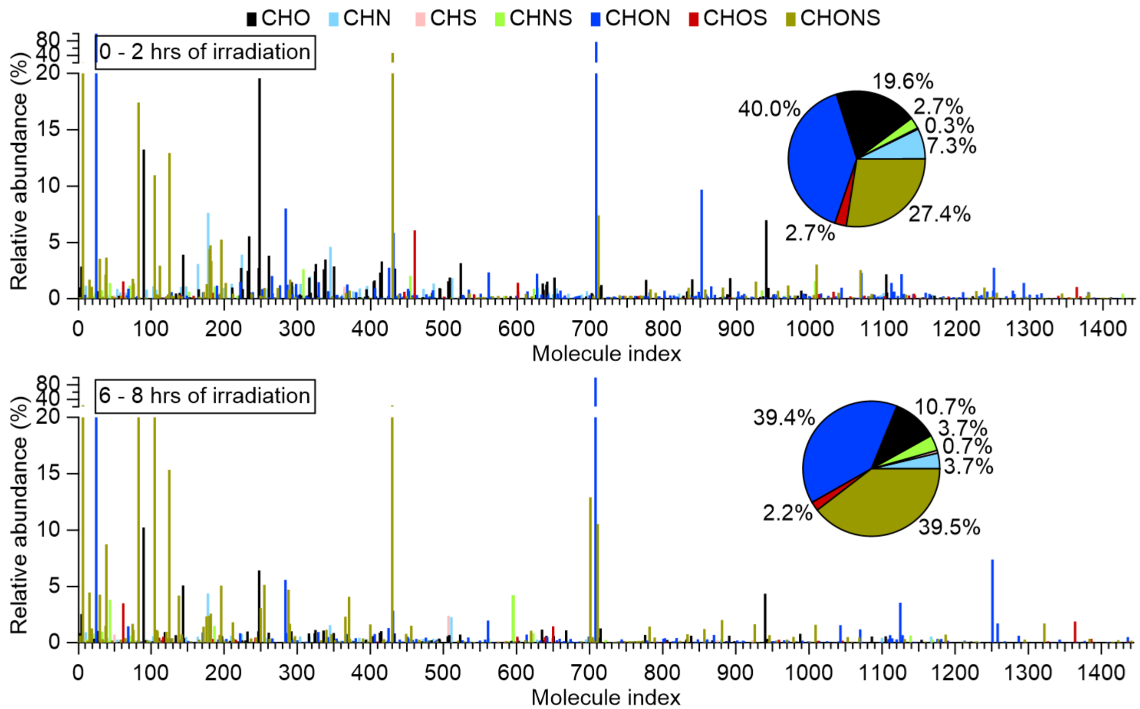

Figure S13. Molecular formulas detected by positive-mode ESI-MS in fog water samples collected during 0 – 2 hours (top) and 6 – 8 hours (bottom) of simulated sunlight irradiation. Bars display the relative signal intensities of individual molecular species, color-coded by elemental composition groups: CHO, CHN, CHS, CHNS, CHON, CHOS, CHONS. Accompanying pie charts summarize the fractional contributions of each group to the total signal.

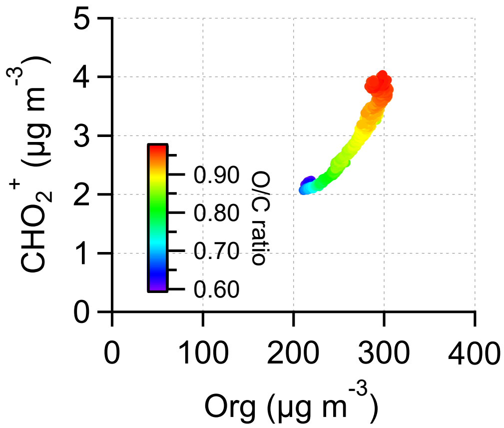

Figure S14. Evolution of AMS-measured CHO_2^+ as a function of organic mass concentration.

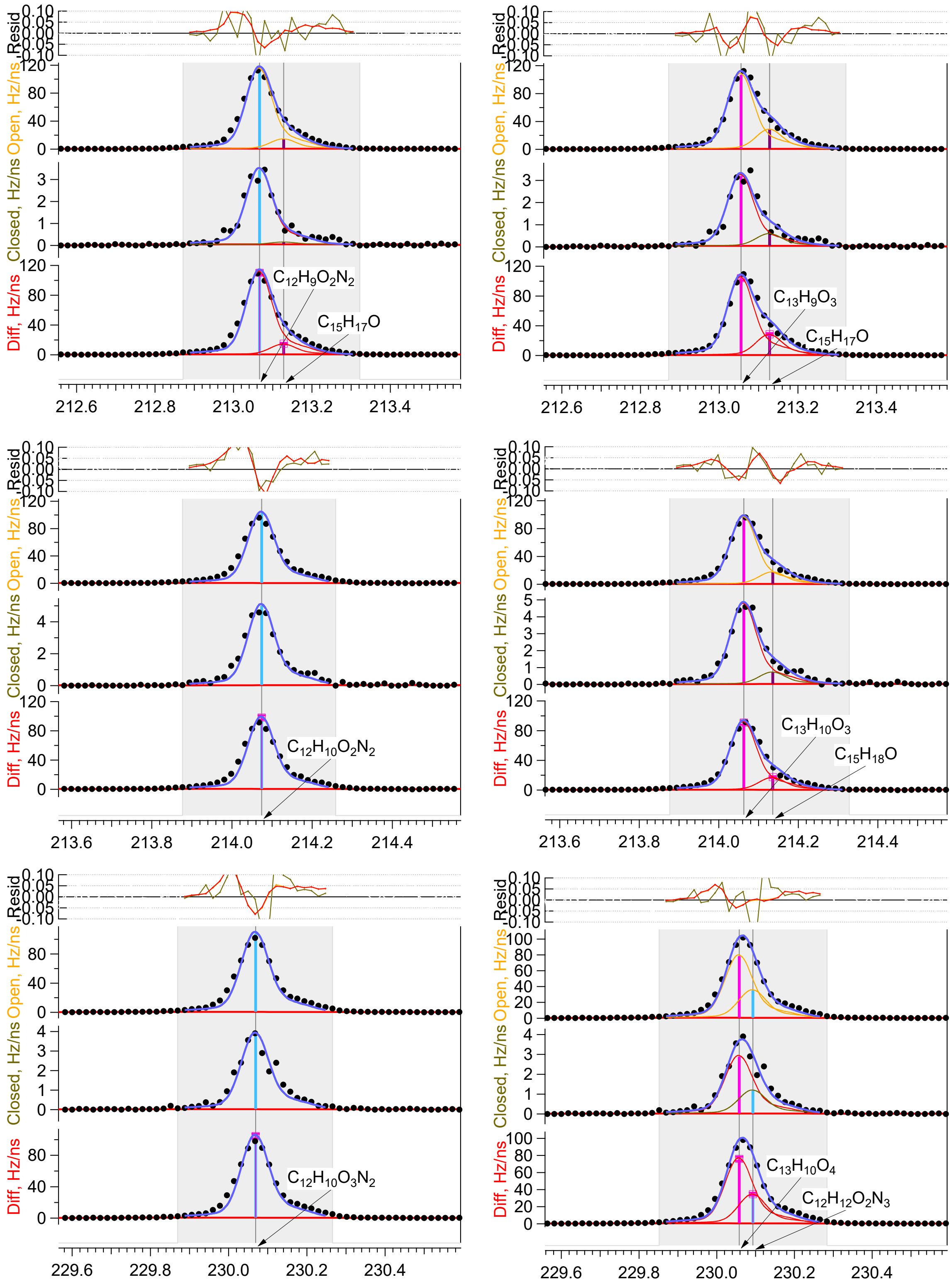
Resid
Open, Hz/ns
Closed, Hz/ns
Diff, Hz/ns
$C_{12}H_9O_2N_2$
$C_{15}H_{17}O$
$C_{13}H_9O_3$
$C_{15}H_{17}O$
$C_{12}H_{10}O_2N_2$
$C_{13}H_{10}O_3$
$C_{15}H_{18}O$
$C_{12}H_{10}O_3N_2$
$C_{13}H_{10}O_4$
$C_{12}H_{12}O_2N_3$
212.6
212.8
213.0
213.2
213.4
213.6
213.8
214.0
214.2
214.4
229.6
229.8
230.0
230.2
230.4

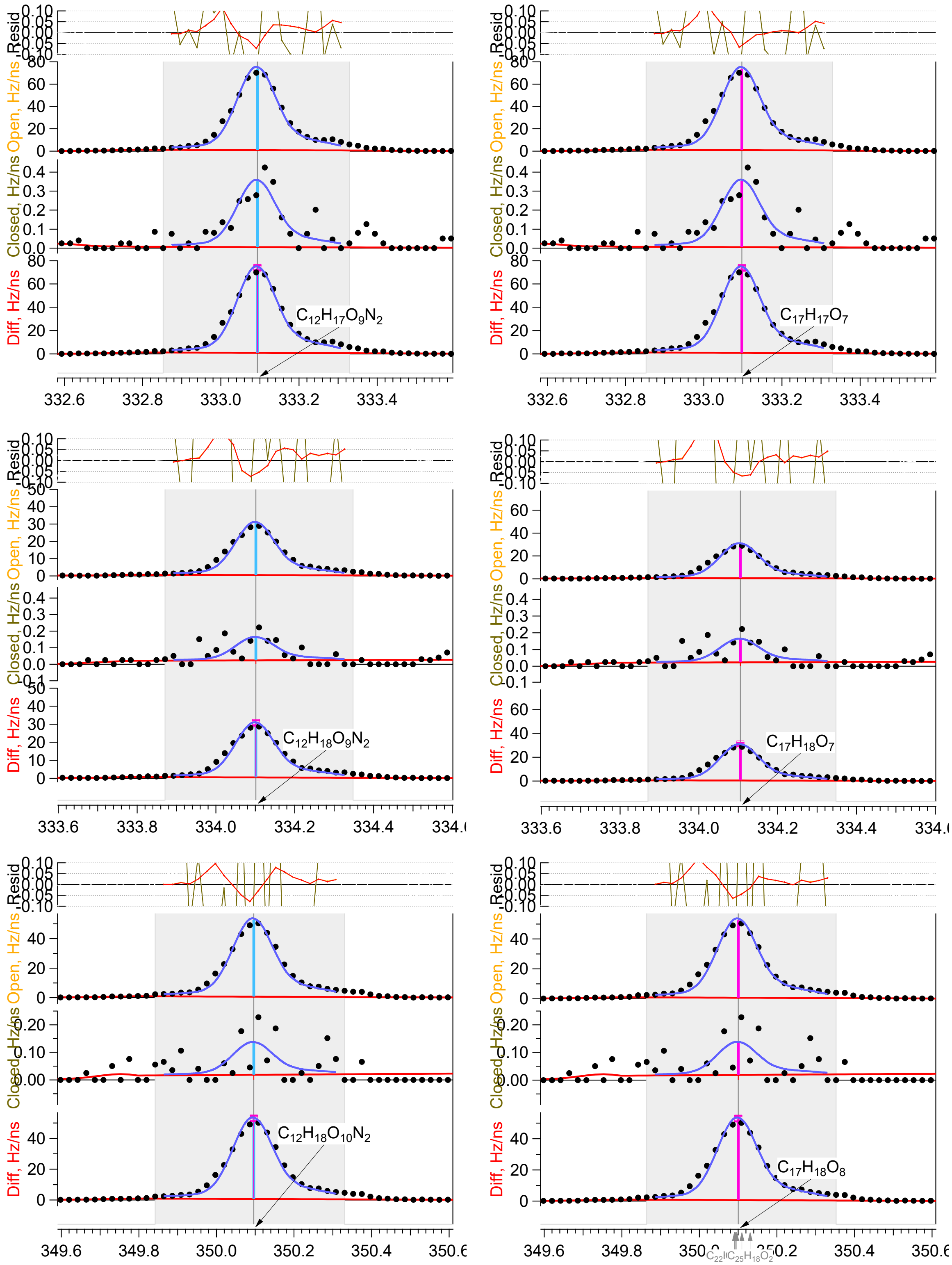

Figure S15. PIKA ion fitting of selected high *m/z* peaks in the HR-AMS spectra of DOM_{OA} at t_{end}. Panels display fitted ion signals at *m/z* 213, 214, 230, 333, 334, and 350. For each m/z, two fits are shown: the left panels assume elemental compositions containing C, H, O and N; the right panels assume compositions with only C, H, and O.

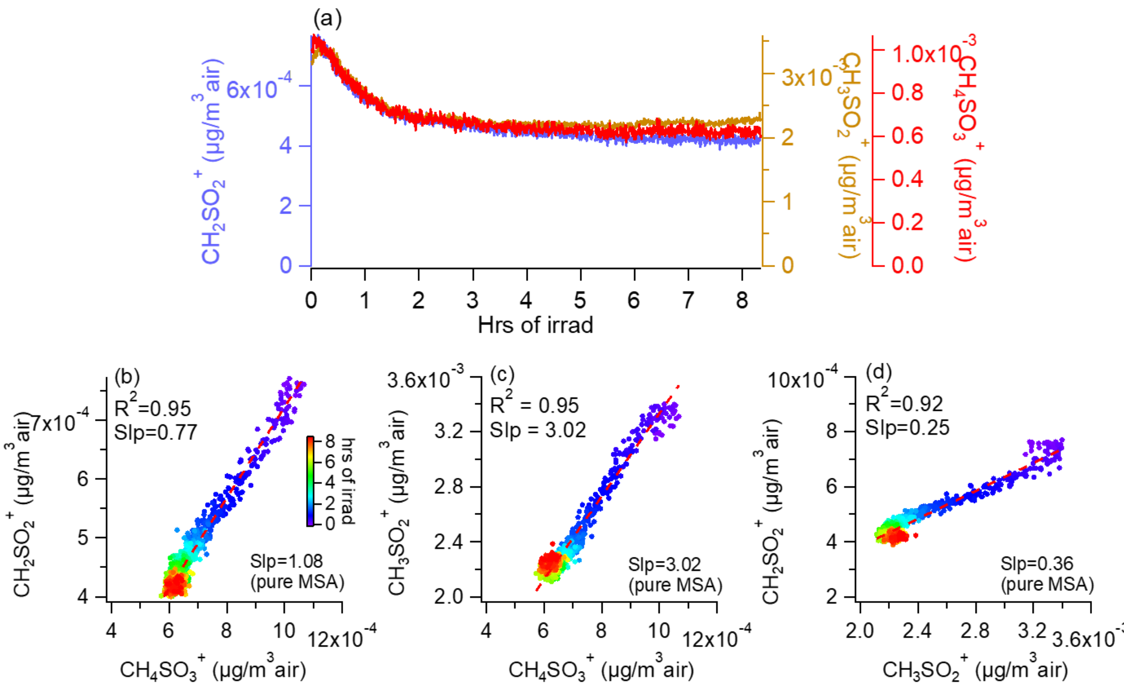

Figure S16. (a) Time trends of HR-AMS tracer ions for MSA (Ge et al., 2012), $CH_2SO_2^+$, $CH_3SO_2^+$, and $CH_4SO_3^+$, during simulated sunlight illumination. **(b -d)** Pairwise correlations among the three ions, with orthogonal distance regression (ODR) slopes (S), intercepts (I), and correlation coefficients (r^2) shown in each panel. Data points are color-coded by hours of illumination (see color bar in b).

References

Ge, X., Zhang, Q., Sun, Y., Ruehl, C. R., and Setyan, A.: Effect of aqueous-phase processing on aerosol chemistry and size distributions in Fresno, California, during wintertime, Environ. Chem., 9, 221–235, 2012.

George, K. M., Ruthenburg, T. C., Smith, J., Yu, L., Zhang, Q., Anastasio, C., and Dillner, A. M.: FT-IR quantification of the carbonyl functional group in aqueous-phase secondary organic aerosol from phenols, Atmos. Environ., 100, 230–237, https://doi.org/10.1016/j.atmosenv.2014.11.011, 2015.

Jiang, W., Misovich, M. V, Hettiyadura, A. P. S., Laskin, A., McFall, A. S., Anastasio, C., and Zhang, Q.: Photosensitized Reactions of a Phenolic Carbonyl from Wood Combustion in the Aqueous Phase—Chemical Evolution and Light Absorption Properties of AqSOA, Environ. Sci. Technol., 55, 5199–5211, https://doi.org/10.1021/acs.est.0c07581, 2021.

Kim, H., Collier, S., Ge, X., Xu, J., Sun, Y., Jiang, W., Wang, Y., Herckes, P., and Zhang, Q.: Chemical processing of water-soluble species and formation of secondary organic aerosol in fogs, Atmos. Environ., 200, 158–166, https://doi.org/https://doi.org/10.1016/j.atmosenv.2018.11.062, 2019.